Effects of α-cluster potentials for the $^{16}O + ^{16}O$ fusion reaction and S factor

G. Kocak,[1] M. Karakoc,[1] I. Boztosun,[2,*] and A. B. Balantekin[3]
[1]*Department of Physics, Erciyes University, 38039, Kayseri, Turkey*
[2]*Department of Physics, Akdeniz University, 07058, Antalya, Turkey*
[3]*Department of Physics, University of Wisconsin, Madison, Wisconsin 53706, USA*
(Received 11 November 2009; published 25 February 2010)

A joint analysis of the elastic-scattering angular distributions and fusion cross sections together with the S factor for the $^{16}O + ^{16}O$ system near and below the Coulomb barrier is reported. To describe these observables within the framework of the optical model, a comparative study of microscopic α-α double-folding clusters and phenomenological shallow potentials with surface-transparent imaginary parts is performed. Although the phenomenological Woods-Saxon type of shallow real potentials is unable to provide a consistent explanation of these data, the α-α double-folding cluster potential obtained by considering the α-cluster structure of ^{16}O provides a considerable improvement. The α-α double-folding cluster potential also reproduces the normalized resonant energy states of ^{32}S for the $N = 24$ cluster band.

DOI: 10.1103/PhysRevC.81.024615 PACS number(s): 25.70.Jj, 24.10.Ht, 24.10.Eq

I. INTRODUCTION

Fusion reactions at energies near and below the Coulomb barrier are being studied both experimentally and theoretically for numerous systems with stable as well as unstable beams. Studies with stable beams, especially for the $^{12}C + ^{12}C$, $^{12}C + ^{16}O$, and $^{16}O + ^{16}O$ systems, are of special interest from an astrophysical point of view, as reliable extrapolation to energies far below the Coulomb barrier is very important for stellar reactions and nucleosynthesis [1]. Such fusion reactions have been studied with several models: A simple one-dimensional barrier penetration model was first used for many systems [2], however, the need to include internal degrees of freedom in this approach has been demonstrated by measurements of the subbarrier fusion [3]. A potential inversion method has been applied to determine the inter-nucleus potential between colliding nuclei [4–6]. In the latter approach, experimental data for heavy-ion fusion cross sections at energies well below the Coulomb barrier were inverted to determine directly the inter-nucleus potential within the framework of the WKB approximation. In another attempt for the $^{16}O + ^{16}O$ system, the ion-ion potential was derived by Reinhard *et al.* from the adiabatic time-depenent Hartree-Fock calculation [7].

The optical model and coupled-channels methods have been widely used for fusion cross-section calculations [8–10]. The coupled-channels formalism, which includes coupling between the relative motion and the internal degrees of freedom such as rotational and vibrational states of the interacting nuclei, has been applied to explain the experimental fusion data [11,12]. Channel coupling effects in the subbarrier fusion of oxygen isotopes with other oxygen isotopes have been explored by Wu *et al.* [13] using data from Ref. [14]. In the coupled-channels formalism, the fusion cross sections are usually calculated either using an incoming wave boundary condition (IWBC) or using an imaginary potential. In the IWBC method, the fusion process is determined by the boundary conditions inside the Coulomb barrier and the imaginary potential has to be within the barrier with a short-range radius, $r \approx 1.0$ fm [15]. These conditions show that fusion strongly depends on the Coulomb barrier. The coupled-channels formalism is the most accepted and utilized model for low-energy fusion reactions, but the outstanding problem for this model is to obtain an explanation of the reaction observables such as the elastic, quasielastic, and fusion data using the same potential [11]. In a previous study, Michaud [16] carried out optical model calculations with a shallow potential containing a soft repulsive core for the $^{12}C + ^{12}C$, $^{12}C + ^{16}O$, and $^{16}O + ^{16}O$ systems and used a weak short-range imaginary potential to explain the fusion data. Recently, Esbensen *et al.* [17–19] examined the fusion cross sections for the $^{16}O + ^{16}O$ system by using a proximity-type potential. In this approach, a shallow real potential constructed from the double-folding (DF) model with a repulsive term is used to explain the fusion data. These studies indicate that shallow potentials are more favorable than deep microscopic or phenomenological potentials. However, the question whether or not these potentials could explain the individual elastic-scattering angular distributions is still unanswered.

In this respect, a long-standing problem in the study of fusion is to understand why different values of surface diffuseness parameters in the nuclear potential are needed to explain elastic-scattering and fusion data. The value of diffuseness to fit fusion data is approximately 1.5 to 2 times larger than the value required to fit elastic-scattering data. Therefore, the same phenomenological Woods-Saxon potential fails to reproduce both these observables [20,21].

In this study, an α-α double-folding cluster (DFC) potential was constructed to investigate this problem. We aim to explain the fusion cross sections, astrophysical S factor, and angular distribution for the $^{16}O + ^{16}O$ system by using the microscopic α-α DFC and compare the results with the phenomenological potentials within the framework of the optical model. We discuss the importance of the diffusion parameter in the surface-transparent imaginary potential of the

*boztosun@akdeniz.edu.tr

phenomenological and microscopic approaches and examine whether it is possible to explain the elastic-scattering angular distribution, fusion cross section, and S-factor experimental data simultaneously.

In Sec. II, we introduce the optical model and the phenomenological and microscopic potentials used to analyze the experimental data on the $^{16}O + ^{16}O$ system. We report the results of these analyses in Sec. III. Section IV is devoted to a summary.

II. THE OPTICAL MODEL

In the optical model, the total potential $V_{\text{total}}(r)$ consists of

$$V_{\text{total}}(r) = V_{\text{Nuclear}}(r) + V_{\text{Coulomb}}(r) + V_{\text{Centrifugal}}(r). \quad (1)$$

The Coulomb and centrifugal potentials are well-known. Owing to a charge $Z_P e$ interacting with a charge $Z_T e$ distributed uniformly over a sphere of radius R_c, the Coulomb potential [22] is

$$\begin{aligned} V_{\text{Coulomb}}(r) &= \frac{1}{4\pi\varepsilon_\circ}\frac{Z_P Z_T e^2}{r}, \quad r \geqslant R_c, \\ &= \frac{1}{4\pi\varepsilon_\circ}\frac{Z_P Z_T e^2}{2R_c}\left(3 - \frac{r^2}{R_c^2}\right), \quad r < R_c, \end{aligned} \quad (2)$$

where R_c is the Coulomb radius, and Z_P and Z_T denote the charges of the projectile P and the target nuclei T, respectively. The centrifugal potential is

$$V_{\text{Centrifugal}}(r) = \frac{\hbar^2 l(l+1)}{2\mu r^2}, \quad (3)$$

where μ is the reduced mass of the colliding pair.

To make a comparative study of this reaction, we use two different potentials for the real part of the optical model potential: One is a phenomenological shallow potential and the other is the microscopic α-α DFC potential. We provide the details of nuclear potentials in the following sections.

A. Phenomenological Potential

For the phenomenological potential, we used the Woods-Saxon shaped potential of Esbensen *et al.* [19], with the same shape and parameters for the real part. This potential is

$$\begin{aligned} V_{\text{Nuclear}}(r) = &\frac{-V_0}{1+\exp[(r-R_V)/a_V)]} \\ &+ i\frac{-W_0}{1+\exp[(r-R_W)/a_W]}, \end{aligned} \quad (4)$$

where $V_0 = 42.14$ MeV, $R_V = r_V(A_P^{1/3} + A_T^{1/3})$ with $r_V = 1.217$ fm, and $a_V = 0.602$ fm. The imaginary part of the potential has the same Woods-Saxon volume shape as in Eq. (4) and its parameters are listed in Table I. The Coulomb potential [23,24] is distributed uniformly over a sphere of radius $R_C = 5.54$ fm.

TABLE I. Parameters of the real and imaginary potentials of the optical model. All imaginary potentials have a Woods-Saxon volume shape.

Potential type	N_R	V_0 (MeV)	r_V (fm)	a_V (fm)	W_0 (MeV)	r_W (fm)	a_W (fm)
α-α DFC	0.897	–	–	–	4.0	1.0	0.35
Woods-Saxon	–	42.14	1.217	0.602	4.0	1.0	0.35

B. α-α Double-Folding Cluster Potential

The numbers of neutrons and protons in the nucleus we study in this paper are integer multiples of those of an α particle, and such nuclei can demonstrate an α-cluster structure [25–28]. Therefore, it will be interesting to obtain the interaction potential by considering the α-particle structure of ^{16}O. To do this, it is presumed [28–30] that (i) the α particles in the nucleus are regarded as elementary bosons, and (ii) each α particle in the nucleus moves independently in a mean field with a repulsive core. As a result, the ground-state wave function of the ^{16}O nucleus can be written as

$$\chi(\vec{r}_1, \vec{r}_2, \vec{r}_3, \vec{r}_4) = \phi_0^{(\alpha)}(\vec{r}_1)\phi_0^{(\alpha)}(\vec{r}_2)\phi_0^{(\alpha)}(\vec{r}_3)\phi_0^{(\alpha)}(\vec{r}_4), \quad (5)$$

where $\phi_0^{(\alpha)}(\vec{r}_i)$ is the lowest orbital wave function of an α particle consisting of $1s$ and $2s$ harmonic-oscillator wave functions. The α-α DFC potential is thus constructed in a similar way to the ordinary DF potential, which is based on the following nucleon-nucleon (NN) interaction, folded with nuclear matter densities of both projectile and target nuclei:

$$\begin{aligned} v_{nn}(r) = &\, 7999\frac{\exp(-4r)}{4r} - 2134\frac{\exp(-2.5r)}{2.5r} \\ &+ J_{00}(E)\delta(r)\ \text{MeV}. \end{aligned} \quad (6)$$

In the present α-α DFC potential, we fold an α-α effective interaction with α-cluster distribution densities and formulate the nucleus-nucleus DFC optical model potential [31] as

$$V_{\text{DFC}}(\vec{r}) = \iint \rho_{cP}(\vec{r}_1)\rho_{cT}(\vec{r}_2)v_{\alpha\alpha}(|\vec{r} + \vec{r}_2 - \vec{r}_1|)d\vec{r}_1 d\vec{r}_2, \quad (7)$$

where ρ_{cP} and ρ_{cT} are the α-cluster distributions for the projectile and target nuclei and $v_{\alpha\alpha}$ is the effective α-α interaction.

The matter distribution of ^{16}O can be parametrized as

$$\rho_M(\vec{r}) = \rho_{0M}(1 + wr^2)\exp(-\beta r^2). \quad (8)$$

This is a modified form of the Gaussian shape for the ρ_M, projectile, and target densities, where $w = \alpha/a^2$ and $\beta = 1/a^2$. The parameter a is the length of the harmonic well and $\alpha \equiv (Z-2)/3$ is proportional to the number of protons in the $1p$ shell; their values are 1.76 and 2.0 fm, respectively [32].

Satchler and Love [33] assumed a Gaussian form for the α-density distribution with a range determined to give the best value [34] of the root mean square (rms) charge radius of 1.67 fm. The corresponding α density is

$$\rho_\alpha(\vec{r}) = \rho_{0\alpha}\exp(-\lambda r^2). \quad (9)$$

TABLE II. Parameters of nuclear matter densities and rms radii of ^{16}O and ^{4}He [31–33].

Nucleus	ρ_0 (fm^{-3})	w (fm^{-2})	$\beta(\lambda)$ (fm^{-2})	$\langle r^2\rangle^{1/2}$ (fm)
^{16}O	0.13173	0.6457	0.3228	2.640
^{4}He	0.4229	0	0.7024	1.461

The parameters for $\rho_{0\alpha}$, ρ_{0M}, w, β, and λ used in Eqs. (8) and (9) are given in Table II.

If ρ_c is the α-cluster distribution function inside the nucleus, then we can relate the nuclear matter density distribution function of the nucleus, ρ_M, to that of the α-particle nucleus, ρ_α, as

$$\rho_M(\vec{r}) = \int \rho_c(\vec{r'})\rho_\alpha(|\vec{r} - \vec{r'}|)d\vec{r'}. \tag{10}$$

Because the densities of the nucleus and the α particle can be calculated from Eqs. (8) and (9), by using Fourier transform techniques [33] for Eq. (10), we can obtain the α-cluster distribution function ρ_c as

$$\rho_c(\vec{r'}) = \rho_{0c}(1 + \mu r'^2)\exp(-\xi r'^2), \tag{11}$$

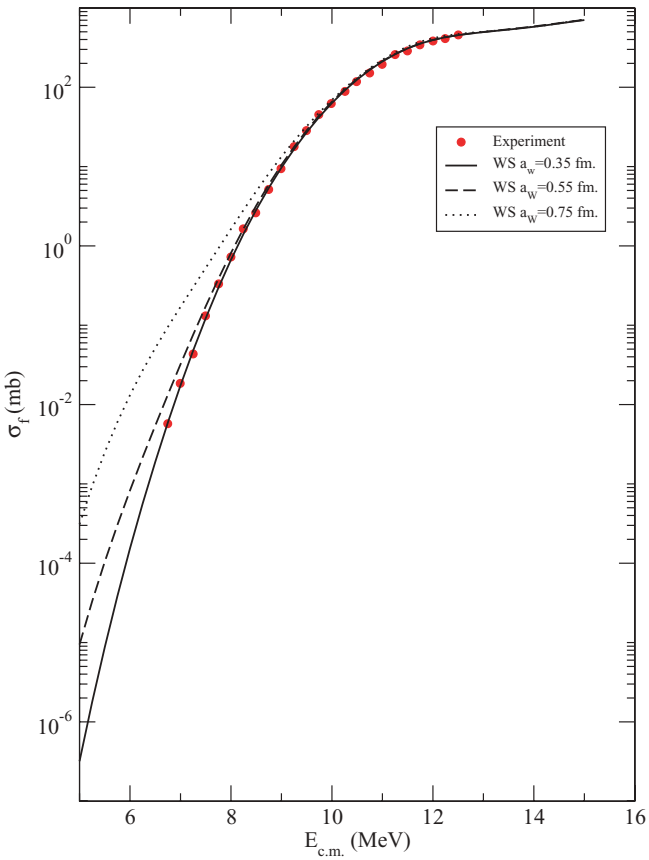

FIG. 1. (Color online) Results of the fusion cross sections for the phenomenological Woods-Saxon (WS) potential obtained using different imaginary diffusion parameters. Experimental data were taken from Ref. [45].

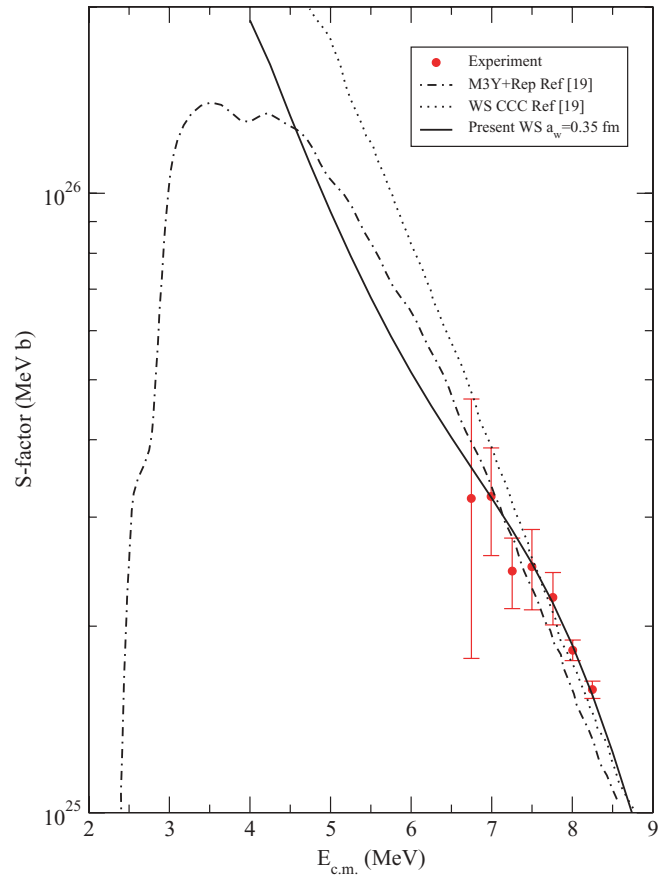

FIG. 2. (Color online) Comparative S-factor results for different calculations. The solid line indicates the present results, and filled circles the experimental data [45], in comparison with the other results taken from Ref. [19].

with

$$\eta = \lambda - \beta, \quad \xi = \beta\lambda/\eta, \quad \mu = \frac{2w\lambda^2}{\eta(2\eta - 3w)}. \tag{12}$$

Several theoretical and experimental efforts have attempted to describe the α-α effective interaction. So far, at least three approaches have been used to analyze the low-energy α-α elastic-scattering data with a purely attractive local, angular-momentum, and energy-independent α-α potential [35–37]. A phenomenological α-α potential including a short-range repulsive and a long-range attractive part have also been used [38,39]. Satchler and Love [33] have calculated an α-α DFC potential based on an M3Y NN effective interaction involving an exchange contribution for the energies of $\sim$10 MeV per nucleon. The resulting potential, which is also purely attractive, is very similar to that of Buck *et al.* [36].

Among these potentials, the α-α potential of Buck *et al.* [36] is the most favorable and the simplest considered in our calculations. This α-α effective interaction potential is given as

$$v_{\alpha\alpha}(r) = -122.6225\exp(-0.202r^2). \tag{13}$$

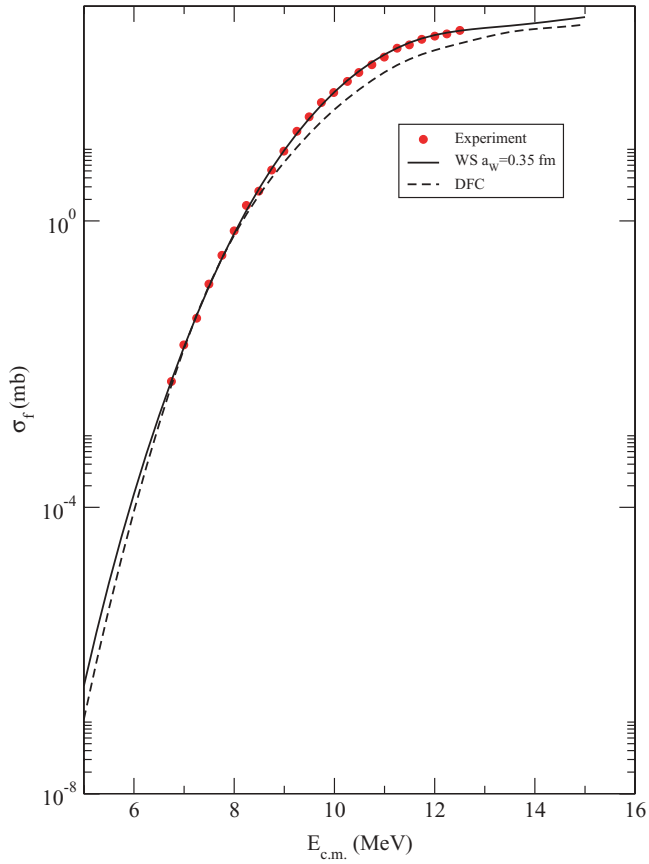

FIG. 3. (Color online) Results of the phenomenological Woods-Saxon and α-α double-folding cluster potentials for the $^{16}O + ^{16}O$ fusion reaction.

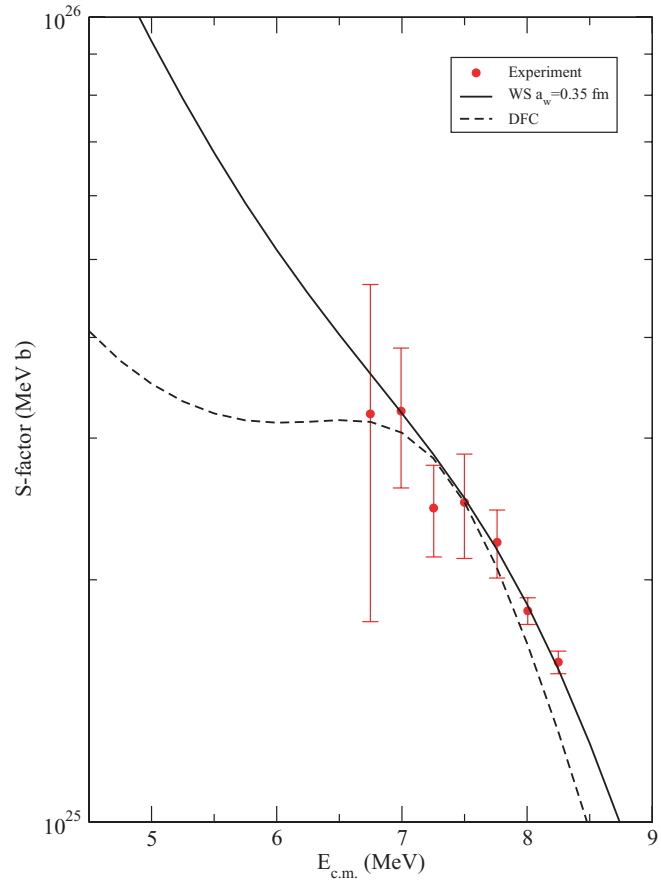

FIG. 4. (Color online) S-factor results for the $^{16}O + ^{16}O$ system obtained using the phenomenological Woods-Saxon and α-α double-folding cluster potentials.

Therefore, the α-α DFC potential consists of a real and an imaginary part as in Eq. (14).

$$V_{\text{Nuclear}}(r) = N_R V_{\text{DFC}}(r) + i \frac{-W_0}{1 + \exp[(r - R_W)/a_W]}. \quad (14)$$

The parameters of the real and imaginary potentials are reported in Table I. The Coulomb radius is taken as $R_C = 5.54$ fm for α-α DFC potentials. The code DFPOT [40] was used for microscopic DF potential calculation and the code FRESCO [41] was used to obtain all reaction observables.

III. RESULTS

We first used the phenomenological Woods-Saxon potential to analyze the fusion cross sections of the $^{16}O + ^{16}O$ system. The parameters in Ref. [19] were used for the real part of the phenomenological potential, together with a weak short-range imaginary potential, which is localized at the Coulomb barrier. As expected we found that the fusion cross section is very sensitive to the value of the diffuseness parameter, whereas the depth and radius of the imaginary potential do not have a large effect on the fusion cross section. The results of the fusion cross-section calculations for the different diffusion parameters are shown in Fig. 1. As shown in Fig. 1, the best result was obtained for $a_W = 0.35$ fm. The other parameters of the phenomenological Woods-Saxon potential are listed in Table I. The theoretical calculation with $a_W = 0.35$ fm is in very good agreement with the experimental data.

The S factor is related to the fusion cross section as

$$S(E) = E\sigma_f \exp(2\pi\eta), \quad (15)$$

where η is the Sommerfeld parameter. The phenomenological Woods-Saxon potential result for the S factor obtained by using the same parameters of the fusion cross-section calculations is shown in Fig. 2. Again, the calculations agree with the data well. In the same figure, we compare our result with that of Esbensen [19], which explains the data by creating a small potential pocket. We observe that the depth of the imaginary potential has a significant impact on the S-factor calculation in contrast to the fusion cross section itself.

Although the phenomenological Woods-Saxon potential approach explains the fusion data together with the S-factor data, it fails to explain the elastic-scattering angular distribution data within the same energy range: When we used the same parameters of the real and imaginary potentials, the oscillatory structure, phase, and magnitude of the elastic scattering data could not be reproduced. This has, nevertheless, been *the* persistent problem (see Refs. [20] and [21]).

We then carried out a comprehensive study of this reaction in a microscopic framework by considering the α-cluster

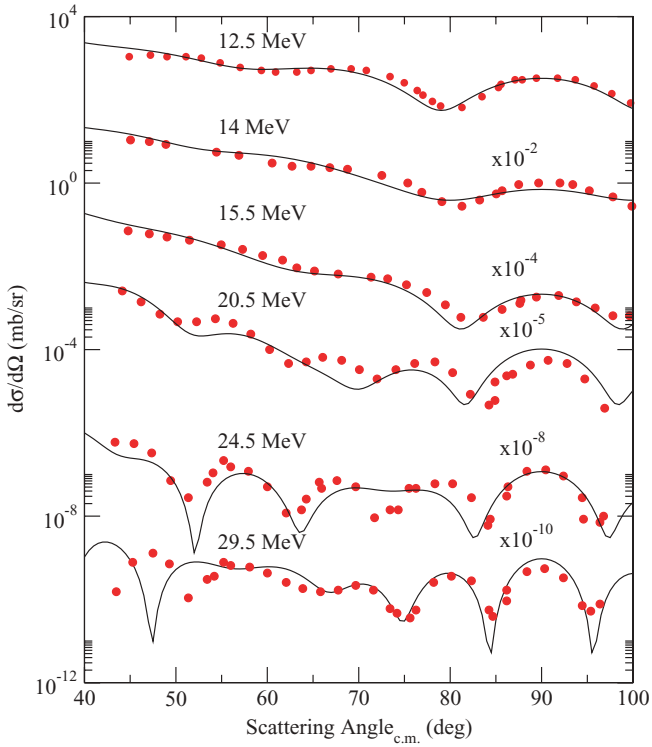

FIG. 5. (Color online) Elastic-scattering angular distributions for the $^{16}O + ^{16}O$ system at different center-of-mass energies. Experimental data (filled circles) were taken from Ref. [46].

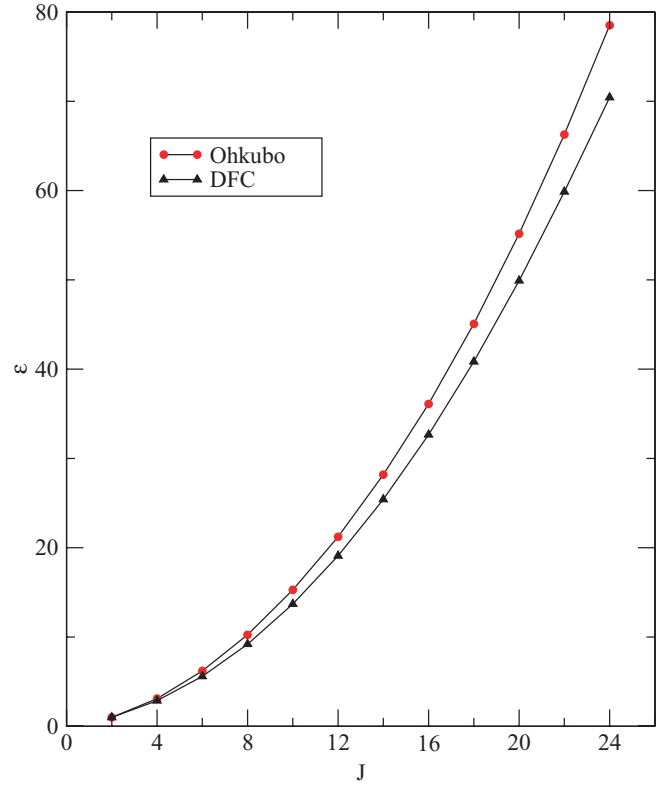

FIG. 6. (Color online) Normalized resonant energy states for the $^{16}O + ^{16}O$ system in comparison with the results of Ohkubo *et al.* [42] obtained using the complex scaling method.

structure of ^{16}O. As explained in Sec. II B, we obtained the real part of the nuclear potential from the α-α DFC and the imaginary part of the nuclear potential from the preceding phenomenological calculation, whose parameters are given in Table I. The value of the normalization (N_R) constant of the α-α DFC potential in this table is determined by requiring that all of the fusion cross sections, S-factor, and elastic-scattering angular distribution data can be described by our calculations.

We present the result of the microscopic potential in the same energy region as the phenomenological potential analysis described previously in Fig. 3. At lower energies there is a reasonable agreement between the fusion cross-section data and the phenomenological Woods-Saxon potential prediction. At energies higher than $E_{c.m.} = 10$ MeV, the microscopic potential underpredicts the fusion cross section in comparison with the experimental data and the theoretical result of the phenomenological Woods-Saxon potential.

In Fig. 4, we present the result of the microscopic α-α DFC potential for the S factor in comparison with the result of the phenomenological Woods-Saxon potential as well as the experimental data. The microscopic potential reproduces the behavior of the S-factor data. With decreasing energy, the microscopic α-α DFC potential result shows a deviation from the results of our phenomenological Woods-Saxon potential and the results of Esbensen [19]. It is clearly shown in Fig. 4 that the microscopic α-α DFC potential predicts the S-factor structure at low energies better than the other approaches.

To explore the elastic-scattering angular distribution of the $^{16}O + ^{16}O$ system, we analyzed the experimental data using the α-α DFC potential with the same parameters used in the fusion cross sections and S-factor calculations. Considerable agreement between our microscopic α-α DFC potential and the experimental data was obtained. The results are shown in Fig. 5. The α-α DFC potential produces the oscillatory structure of the elastic- scattering angular distributions data with correct phases and magnitudes. We point out that small changes in the normalization constant N_R could further improve the agreement between the theoretical results and the experimental data.

To summarize, it seems that the microscopic α-α DFC potential provides a simultaneous explanation of the fusion, S-factor, and elastic-scattering angular distribution data in a unified way. To see the validity of the α-α DFC potential for resonant and bound states from the nuclear structure viewpoint, we also calculated the normalized resonant energy states for the $N = 24$ cluster band that was investigated by Ohkubo *et al.* [42] using a complex scaling method. In Fig. 6, we show the results obtained using the code GAMOW [43]. In this figure, the normalized resonant energy states were calculated using the following equation:

$$\varepsilon = \frac{E(J^+) - E(0^+)}{E(2^+) - E(0^+)}. \tag{16}$$

Our results show the same behavior as the results of Ref. [42] for the $N = 24$ cluster band of the ^{32}S nucleus.

IV. SUMMARY AND CONCLUSIONS

In this paper, we have focused on explaining the fusion, the *S*-factor, and the elastic-scattering angular distribution data of the $^{16}O + ^{16}O$ system within the framework of the *same* optical model. We have utilized both phenomenological and microscopic potentials. In the first part of this paper, to describe fusion, *S*-factor and elastic-scattering angular distribution data simultaneously, we have used a phenomenological Woods-Saxon potential approach with a weak short-range imaginary potential. As in the previous work, we observed that the diffusion parameter of the imaginary potential has a significant effect on the fusion cross-section results. We have determined that the best value that predicts the fusion cross-section data is $a_W = 0.35$ fm. Although this phenomenological Woods-Saxon potential approach explains the fusion and *S*-factor data well, it is unable to provide a reasonable description of the elastic-scattering angular distribution data.

We have then explored the use of the microscopic deep potential obtained by the α-α DFC model. The α-α DFC potential can describe the broad features of the fusion, *S*-factor, and elastic-scattering angular distribution data simultaneously. We emphasize that the same α-α DFC potential also successfully predicts the trend of the normalized resonant energy states for the $N = 24$ cluster band of the ^{32}S nucleus. This study shows the benefits of the α-cluster potential approximation to describe systematically the reaction observables of light-ion interactions such as the $^{16}O + ^{16}O$ system. In contrast, it is pointed out that experimental data for $^{16}O + ^{154}Sm$ quasielastic scattering at backward angles also favor a large value of the surface diffuseness parameter, and a DF approach fails to reproduce the experimental excitation function of quasielastic scattering for this system at energies around the Coulomb barrier [44]. It will be interesting to apply the α-cluster DF approximation to study fusion and scattering observables of other, lighter systems and explore why it seems to describe the data better.

ACKNOWLEDGMENTS

This work was supported in part by Turkish Science and Research Council (TÜBİTAK) Grant Nos. 107T824 and 109T373, Turkish Academy of Sciences (TÜBA-GEBİP), Akdeniz University Scientific Research Projects Unit, and in part by US National Science Foundation Grant No. PHY-0855082 and the University of Wisconsin Research Committee, under funds granted by the Wisconsin Alumni Research Foundation. G. Kocak acknowledges the support from TÜBİTAK Integrated Ph.D. Program Grant No. BİDEB-2219. The authors wish to thank A. Soylu and I. Inci for their help in using the code GAMOW.

[1] L. R. Gasques *et al.*, Phys. Rev. C **76**, 035802 (2007).
[2] A. B. Balantekin and N. Takigawa, Rev. Mod. Phys. **70**, 77 (1998).
[3] M. Beckerman *et al.*, Phys. Rev. Lett. **45**, 1472 (1980).
[4] A. B. Balantekin, S. E. Koonin, and J. W. Negele, Phys. Rev. C **28**, 1565 (1983).
[5] K. Hagino and Y. Watanabe, Phys. Rev. C **76**, 021601(R) (2007).
[6] K. Hagino and N. Rowley, AIP Conf. Proc. **1098**, 18 (2009).
[7] P. G. Reinhard, J. Friedrich, K. Goeke, F. Grummer, and D. H. E. Gross, Phys. Rev. C **30**, 878 (1984).
[8] C. R. Morton, A. C. Berriman, M. Dasgupta, D. J. Hinde, J. O. Newton, K. Hagino, and I. J. Thompson, Phys. Rev. C **60**, 044608 (1999).
[9] K. Hagino, N. Takigawa, M. Dasgupta, D. J. Hinde, and J. R. Leigh, Phys. Rev. C **55**, 276 (1997).
[10] H. Esbensen, C. L. Jiang, and K. E. Rehm, Phys. Rev. C **57**, 2401 (1998).
[11] M. Dasgupta *et al.*, Nucl. Phys. **A787**, 144c (2007).
[12] C. H. Dasso *et al.*, Nucl. Phys. **A405**, 381 (1983).
[13] J. Q. Wu, G. Bertsch, and A. B. Balantekin, Phys. Rev. C **32**, 1432 (1985).
[14] J. Thomas, Y. T. Chen, S. Hinds, K. Langanke, D. Meredith, M. Olson, and C. A. Barnes, Phys. Rev. C **31**, 1980 (1985).
[15] G. R. Satchler, Phys. Rep. **199**, 147 (1991).
[16] G. Michaud, Phys. Rev. C **8**, 525 (1973).
[17] S. Misicu and H. Esbensen, Phys. Rev. C **75**, 034606 (2007).
[18] H. Esbensen and S. Misicu, Phys. Rev. C **76**, 054609 (2007).
[19] H. Esbensen, Phys. Rev. C **77**, 054608 (2008).
[20] A. Mukherjee, D. J. Hinde, M. Dasgupta, K. Hagino, J. O. Newton, and R. D. Butt, Phys. Rev. C **75**, 044608 (2007).
[21] J. O. Newton, R. D. Butt, M. Dasgupta, D. J. Hinde, I. I. Gontchar, C. R. Morton, and K. Hagino, Phys. Rev. C **70**, 024605 (2004).
[22] G. R. Satchler, Nucl. Phys. **A409**, 3c (1983).
[23] G. R. Satchler, *Direct Nuclear Reactions* (Oxford University Press, Oxford, 1983); *Introduction to Nuclear Reactions* (Macmillan, London, 1980).
[24] W. Greiner, J. Y. Park, and W. Scheid, *Nuclear Molecules* (World-Scientific, Singapore, 1995).
[25] W. D. M. Rae, Int. J. Mod. Phys. A **3**, 1343 (1988).
[26] M. Freer and A. C. Merchant, J. Phys. G **23**, 261 (1997); M. Freer, R. R. Betts, and A. H. Wuosmaa, Nucl. Phys. **A587**, 36 (1995).
[27] S. Marsh and W. D. M. Rae, Phys. Lett. **B180**, 185 (1986).
[28] M. Karakoc and I. Boztosun, Phys. Rev. C **73**, 047601 (2006).
[29] Q.-R. Li and Y.-X. Yang, Nucl. Phys. **A561**, 181 (1993).
[30] Y.-X. Yang and Q.-R. Li, Phys. Rev. C **72**, 054603 (2005).
[31] M. El-Azab Farid, Z. M. M. Mahmoud, and G. S. Hassan, Nucl. Phys. **A691**, 671 (2001).
[32] H. F. Ehrenberg *et al.*, Phys. Rev. **113**, 666 (1959).
[33] G. R. Satchler and W. G. Love, Phys. Rep. **55**, 183 (1979).
[34] J. S. McCarthy *et al.*, Phys. Rev. C **15**, 1396 (1977).
[35] V. G. Neudatchien, V. I. Kukulin, V. L. Korotkikh, and V. P. Korennoy, Phys. Lett. **B34**, 581 (1971).
[36] B. Buck, H. Friedrich, and C. Wheathly, Nucl. Phys. **A275**, 246 (1977).
[37] L. Marquez, Phys. Rev. C **28**, 2525 (1983).
[38] P. Darriulat, G. Igo, H. G. Pugh, and H. D. Holmgren, Phys. Rev. **137**, B315 (1965).
[39] G. Spitz, H. Klar, and E. W. Schmid, Z. Phys. A **322**, 49 (1985).
[40] J. Cook, Comput. Phys. Commun. **25**, 125 (1982).

[41] I. J. Thompson, Comput. Phys. Rep. **7**, 167 (1988).
[42] S. Ohkubo and K. Yamashita, Phys. Rev. C **66**, 021301(R) (2002) .
[43] T. Vertse, K. F. Pal, and Z. Balogh, Comput. Phys. Commun. **27**, 309 (1982).
[44] K. Hagino, T. Takehi, A. B. Balantekin, and N. Takigawa, Phys. Rev. C **71**, 044612 (2005).
[45] J. Thomas, Y. T. Chen, S. Hinds, D. Meredith, and M. Olson, Phys. Rev. C **33**, 1679 (1986).
[46] J. V. Maher *et al.*, Phys. Rev. **188**, 1665 (1969).